J Mater Sci (2009) 44:6644–6653
DOI 10.1007/s10853-009-3510-z

MESOSTRUCTURED MATERIALS

Synthesis, characterization and catalytic activity of Au supported on functionalized SBA-15 for low temperature CO oxidation

M. G. Cutrufello · E. Rombi · C. Cannas · M. Casu · A. Virga · S. Fiorilli · B. Onida · I. Ferino

Received: 28 November 2008 / Accepted: 22 April 2009 / Published online: 7 May 2009

Abstract SBA-15 functionalization with 3-mercaptopropyltrimethoxysilane was used to prepare a supported gold catalyst for the low temperature CO oxidation reaction. Catalytic runs were performed at atmospheric pressure and $T = 40$–150 °C and the influence of different thermal treatments of the sample prior to reaction was studied. The modifications induced by the pre-treatments in the physico-chemical properties of both the carrier and the disperse phase were investigated by chemical analysis, CHS elemental analysis, N_2 adsorption–desorption, X-ray diffraction (XRD), transmission electron microscopy (TEM), solid state cross-polarization magic-angle-spinning nuclear magnetic resonance spectroscopy (CPMAS NMR) of ^{29}Si and ^{13}C and Fourier transform infrared spectroscopy (FTIR). The pre-treatment conditions were found to strongly affect both the gold particle size and the nature of the Au surface species. An appreciable catalytic activity was found on samples treated at 600 °C in H_2/He atmosphere, provided that the functionalizing agent had been completely removed by a previous high-temperature calcination.

M. G. Cutrufello (✉) · E. Rombi · C. Cannas · M. Casu · I. Ferino
Dipartimento di Scienze Chimiche, Università di Cagliari, Complesso Universitario di Monserrato, S.S. 554 bivio per Sestu, 09042 Monserrato, CA, Italy
e-mail: gcutrufe@unica.it

A. Virga · S. Fiorilli · B. Onida
Dipartimento di Scienza dei Materiali e Ingegneria Chimica, Politecnico di Torino, Via Duca degli Abruzzi 24, 10129 Torino, Italy

Introduction

Gold highly dispersed on solid supports has shown unexpectedly high catalytic activity towards different reactions of both industrial and environmental importance. Among them, CO oxidation at low temperature has been extensively studied on gold nanoparticles supported on several oxides [1–14]. It is generally accepted that for high catalytic activities in such reaction the size of supported Au nanoparticles should be below 5 nm [2]. When silica is used as a support, conventional gold deposition methods lead to Au nanocrystals significantly above the critical range (about 20 nm) [4]. A possible way for controlling the gold nanoparticle size might be represented by their confinement within the pores of SBA-15 [15], a mesostructured silica with a highly ordered 2D hexagonal structure, well-defined pore size and thicker walls (which lead to improved hydrothermal and thermal stability) than other mesostructured silicas. In order to increase the metal dispersion on this support, functionalization of its surface by organo-silane molecules is necessary [16–20]. Previous results obtained by the present authors [20] showed that gold supported on SBA-15 functionalized with 3-mercaptopropyltrimethoxysilane (MPTMS) by a co-condensation or a post-synthesis method was active at low temperature only when submitted to high-temperature calcination in air followed by treatment under H_2/He atmosphere. Similar results had previously been reported by other authors [12]. It seems that the first step is necessary to completely eliminate the functionalizing agent, whereas the H_2/He treatment would induce the formation on the silica support of electron-rich defects (E' centres) responsible for oxygen adsorption. It was also found [20] that gold plays a key role in assisting the formation of E' centres on the silica surface; interestingly, the turnover frequencies for CO

oxidation were quite high in spite of the (relatively) large size of the Au particles (ca. 6 nm).

In the present work the Au/SBA-15 system is further investigated. Gold was deposited on SBA-15 functionalized by a post-synthesis procedure. The catalyst was submitted to different thermal treatments, namely: calcination in air, treatment under H_2 atmosphere, calcination followed by H_2 treatment. The effect of a thermal cycle involving H_2 treatment/calcination/H_2 treatment on the size of the Au particles was also checked. The resulting samples were thoroughly characterized by chemical analysis, elemental analysis (CHS), nitrogen physisorption, X-ray diffraction (XRD), transmission electron microscopy (TEM), solid state CPMAS NMR. The Au–CO interaction was investigated by FTIR spectroscopy. Catalytic testing was carried out at atmospheric pressure in the 40–150 °C range.

Experimental

Materials

Tetraethylorthosilicate (TEOS, 98%), pluronic copolymer P123 ($EO_{20}PO_{70}EO_{20}$), 3-mercaptopropyltrimethoxysilane (MPTMS, 95%), *p*-toluenesulphonic acid monohydrate (98%), toluene (99.8%), *N*,*N*-dimethylformamide (99.8%), diethylether (≥98%), dichloromethane (≥99.5%) and NH_4F (≥98%) were supplied by Aldrich; Na citrate (≥99%), $NaBH_4$ (≥96%), $HAuCl_4$ (Au≥49%) and ethanol (96%) were supplied by Fluka; HCl (37%) was provided by Merck. All the materials were reagent grade.

Catalyst preparation

Mesostructured silica SBA-15 was synthesized according to [15]. The functionalized sample (SBA-15-SH) was obtained by addition of a proper amount of MPTMS (MPTMS/SBA-15 molar ratio = 0.5) to a suspension of freshly evacuated (150 °C, 10^{-1} Torr, 12 h) SBA-15 (1 g) in toluene (20 mL). After 30 min under stirring, appropriate amounts of water (H_2O/MPTMS molar ratio = 1), *p*-toluenesulphonic acid (acid/MPTMS molar ratio = 0.05) and NH_4F (NH_4F/MPTMS molar ratio = 0.05) were added to the suspension. *p*-Toluenesulphonic acid catalyses the hydrolysis of the alkoxy-silane molecules and prevents their condensation, favouring the reaction of the functionalizing agent with the silica surface compared to its undesired polymerization [21, 22]. The suspension was stirred at 25 °C for 1 h and then heated at 60 °C for 6 h and at 120 °C for 1 h. The suspension was then filtered under vacuum and the recovered SBA-15-SH was carefully washed with toluene and dimethylformamide. Removal of the excess organo-silane was achieved by Soxhlet extraction with a diethylether/dichloromethane mixture (1:1) at 70 °C; the solid was finally washed with dichloromethane and dried overnight.

The functionalized support was suspended in 80 mL of distilled water and stirred for 30 min at 80 °C; in order to obtain the desired Au loading (3 wt%), an appropriate amount of an $HAuCl_4$ aqueous solution was added to the suspension which rapidly became colourless, indicating that deposition of gold on the SBA surface had occurred. After 30 min, a proper quantity of sodium citrate (Na citrate/Au molar ratio = 20) was dissolved in 50 mL of distilled water and poured into the mixture. After 20 min, the solid was recovered by filtration and dried at 120 °C for 12 h. Reduction of gold was performed by adding a suitable amount of a 1 wt% $NaBH_4$ solution (in ethanol, $NaBH_4$/Au molar ratio = 10) to the solid suspended in 100 mL of ethanol. After 18 h at 60 °C under stirring, the suspension was filtered and the solid dried at 120 °C overnight after washing with ethanol and water. The resulting sample was named Au/SBA-15-SH.

Characterization

Inductively coupled plasma atomic emission spectrometry (ICP-AES) analysis was performed with a Varian Liberty 200 spectrophotometer to determine the Au content. Au/SBA-15-SH (50 mg) was treated with 12 mL of a nitric and hydrochloric acid mixture (1:3 molar ratio) for 3 h at 80 °C under stirring to extract the metal from the surface. After complete removal of the acid solution by repeatedly washing and evaporating with double-distilled water, the sample was filtered and the liquid was quantitatively recovered and diluted to 250 mL.

Textural analyses were carried out on a Sorptomatic 1990 System (Fisons Instruments), by determining the nitrogen adsorption/desorption isotherms at −196 °C. Before analysis, the samples were heated overnight under vacuum up to 150 °C (heating rate = 1 °C min^{-1}).

CHS analysis was carried out with an EA 1108 CHNS-O analyser (Fisons Instruments) by total combustion of the samples in an oxygen/helium mixture.

High resolution NMR spectra were collected using a Varian UNITY INOVA Spectrometer with a 9.39 T wide-bore Oxford magnet. Experiments were performed with a 4 mm probe and Si_3N_4 rotors at a spinning rate of 7 kHz. ^{13}C CPMAS spectra were collected with a recycle time of 3 s and a contact time of 4 ms. ^{29}Si CPMAS spectra were collected with a recycle time of 4 s and a contact time of 4 ms. ^{29}Si and ^{13}C chemical shifts were referenced to that of tetramethylsilane.

Structural evolution of the samples was monitored by XRD using a Seifert diffractometer with a θ–θ Bragg Brentano geometry with Cu-Kα wavelength. The mean dimension of crystallites was obtained by the Scherrer equation with the Warren correction [23].

Sample powders were observed in electron micrographs obtained by a transmission electron microscope (JEOL 200CX) operating at 200 kV. Finely ground samples were dispersed in n-octane and subjected to an ultrasonic bath. The suspensions were then dropped on carbon-coated copper grids for the observation.

FTIR spectra were collected on a Bruker FTIR Equinox 55 equipped with a MCT cryodetector working at 2 cm^{-1} resolution. The interaction with CO was followed at the nominal temperature of −196 °C by using liquid nitrogen as a coolant. Thin self-supporting wafers were prepared and submitted to the following thermal treatments: (a) calcination in O_2 (200 Torr) at 560 °C (heating rate 2 °C min^{-1}) for 6 h, (b) treatment in H_2 (200 Torr) at 600 °C (heating rate 2.5 °C min^{-1}) for 2 h, (c) calcination in O_2 (200 Torr) at 560 °C (heating rate 2 °C min^{-1}) for 6 h, followed by treatment in H_2 (200 Torr) at 600 °C (heating rate 2.5 °C min^{-1}) for 2 h, (d) treatment in H_2 (200 Torr) at 600 °C (heating rate 2.5 °C min^{-1}) for 2 h, followed by calcination in O_2 (200 Torr) at 560 °C (heating rate 2 °C min^{-1}) for 6 h and a further treatment in H_2 (200 Torr) at 600 °C (heating rate 2.5 °C min^{-1}) for 2 h.

Catalytic tests

Catalytic runs were performed in a quartz-glass continuous-flow fixed-bed microreactor at atmospheric pressure, in the temperature range 40–150 °C, by contacting 30 mg of catalyst with a CO/O_2 mixture (total flow = 55 mL min^{-1}; 1.5 vol% CO, 1.5 vol% O_2, balance He). Analyses of the reaction mixture were performed on-line with a HP 6890 GC, equipped with a HP Poraplot Q capillary column and a TCD. For each reaction temperature, samples were collected after 60 min on stream to allow the attainment of steady-state conditions. Prior to reaction, the catalyst was submitted to diverse thermal treatments: (i) calcination in flowing air at 560 °C for 6 h (heating rate, 2 °C min^{-1}; flow rate, 15 mL min^{-1}); (ii) treatment in a H_2 (5 vol%)/He mixture at 600 °C for 1 h (heating rate, 5 °C min^{-1}; flow rate, 140 mL min^{-1}); (iii) calcination in air at 560 °C and subsequent treatment under H_2 (5 vol%)/He atmosphere at 600 °C; (iv) treatment in a H_2 (5 vol%)/He mixture at 600 °C, calcination in air at 560 °C and further treatment under H_2 (5 vol%)/He atmosphere at 600 °C. Catalytic results are expressed in terms of CO conversion ($mol_{CO\text{-}reacted}\ mol^{-1}_{CO\text{-}fed}$ 100) and turnover frequency (TOF, $mol_{CO\text{-}reacted}\ mol^{-1}_{surface\text{-}Au}\ s^{-1}$).

Results and discussion

Structural and textural features of SBA-15, SBA-15-SH and as-made Au/SBA-15-SH

The low angle X-ray diffraction (LA-XRD) patterns of SBA-15, SBA-15-SH and as-made Au/SBA-15-SH are reported in Fig. 1. The SBA-15 sample (Fig. 1a) shows three well-resolved diffraction peaks which can be indexed as the (100), (110) and (200) reflections typical of the 2D hexagonal mesostructure (space group P6mm). TEM imaging was carried out to investigate the internal architecture of the SBA-15 sample. With the viewing direction parallel (Fig. 2a) or perpendicular (Fig. 2b) to the main axis of the pores, the highly ordered 2D hexagonal regularity is confirmed. The ordered arrays of silica channels have a mean diameter of about 6–7 nm with a wall thickness of ca. 3 nm. The low angle X-ray diffraction pattern of the SBA-15-SH sample (Fig. 1b) is similar to that of the parent SBA-15, though the weak (110) and (200) diffraction peaks are less intense. A slight shift of the reflections towards lower angles is observed, which has recently been reported also by other authors [24, 25]. A corresponding increase in the lattice constant from 9.5 to 9.7 nm can be

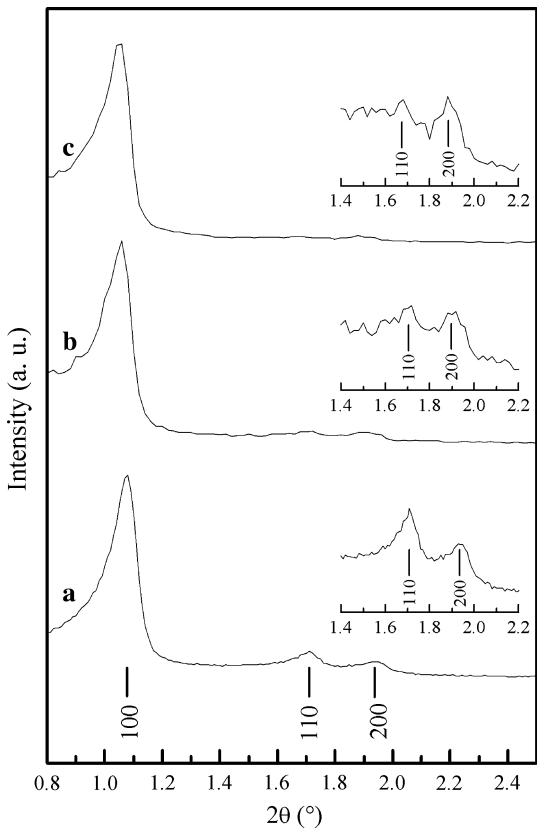

Fig. 1 Low angle X-ray diffraction patterns: SBA-15 (*a*), SBA-15-SH (*b*), as-made Au/SBA-15-SH (*c*)

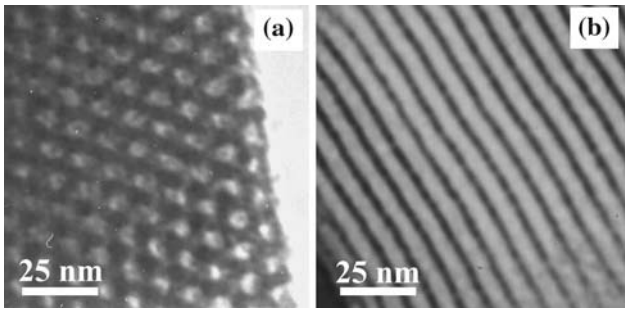

Fig. 2 TEM micrographs of SBA-15

calculated. This indicates that changes in the pore size and/or the wall thickness have occurred as a consequence of the functionalization process. No changes (Fig. 1c) in the LA-XRD pattern are observed after gold loading (2.97 wt%, determined experimentally).

The N_2 adsorption–desorption isotherms and the pore size distribution curves (inset) of the samples are shown in Fig. 3. The pure support exhibits a type IV isotherm with an H1 hysteresis loop starting from $P/P_0 \cong 0.60$, typical of the SBA-15 structure. A surface area (S_{BET}) of 1047 $m^2\ g^{-1}$ and a pore volume (V_p) of 1.83 $cm^3\ g^{-1}$ were calculated from the BET equation. By applying the BJH method to the desorption branch of the curve, a narrow pore size distribution, centred at 6.8 nm, was obtained. A wall thickness of 2.7 nm was calculated from the

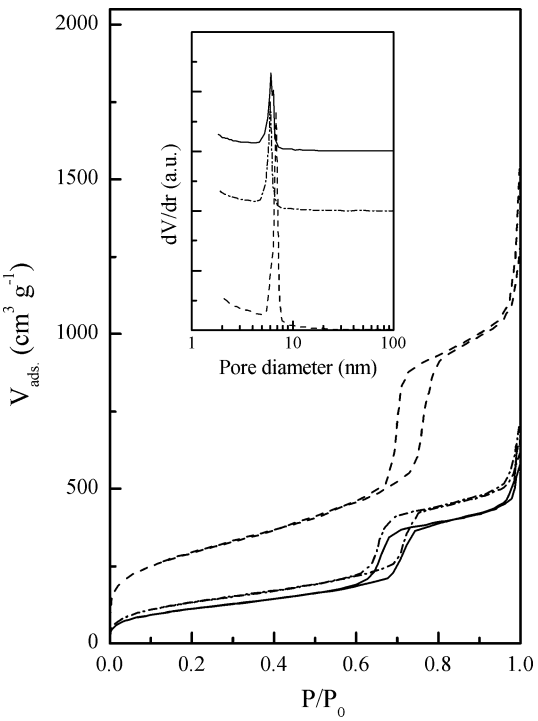

Fig. 3 N_2 adsorption–desorption and pore size distribution curves: SBA-15 (*dash line*), SBA-15-SH (*dash-dot line*), as-made Au/SBA-15-SH (*solid line*)

difference between the lattice parameter determined by X-ray diffraction and the pore size obtained by nitrogen adsorption–desorption analysis [26]. Both the pore size and the wall thickness values are in agreement with those obtained from TEM. Figure 3 shows that the introduction of MPTMS into the SBA-15 pores results in a decrease in S_{BET} (491 $m^2\ g^{-1}$), V_p (0.90 $cm^3\ g^{-1}$) and mean pore diameter (6.0 nm). The wall thickness, calculated as the difference between the lattice parameter and the pore size, is 3.7 nm. Such a decrease in S_{BET} and V_p is too high for resulting only from the presence of MPTMS on the pore walls. Partial pore blockage as well as collapsing (to some extent) of the mesostructure could also be responsible for the observed dramatic surface area and pore volume loss. Loading of SBA-15-SH with gold results in just a slight decrease in both surface area (from 491 to 410 $m^2\ g^{-1}$) and pore volume (from 0.90 to 0.83 $cm^3\ g^{-1}$), the mean pore diameter remaining virtually unchanged (6.1 nm). This is in agreement with LA-XRD data, which showed that the presence of the gold nanoparticles does not significantly affect the features of the support.

To check whether the incorporation of MPTMS in the silica structure actually occurs during the functionalization step, solid state CPMAS NMR of ^{29}Si and ^{13}C experiments were carried out (Fig. 4). The ^{29}Si CPMAS spectrum of SBA-15-SH (Fig. 4a) shows three partially overlapping signals in the region from −80 to −120 ppm, ascribable to Q^2 (−92 ppm), Q^3 (−100 ppm) and Q^4 (−110 ppm) groups [27]. Besides these high field signals, the sample shows peaks at low field in the range from −50 to −75 ppm, which can be assigned to T^2 (−56 ppm) and T^3 (−66 ppm) groups [28, 29], i.e. to the silane organic moieties incorporated as a part of the silica wall structure. The presence of the latter signals demonstrates the successful incorporation of the functional groups into the silica framework. The inclusion of the mercapto-propyl functional groups into the silica network is also confirmed by the ^{13}C CPMAS NMR spectrum of SBA-15-SH (Fig. 4b), which shows the presence of two main peaks at 11.4 and 27.6 ppm. The first is ascribed to the carbon atom C_1 directly bonded to Si, the second is associated to C_2 and C_3 atoms; although CPMAS NMR is not quantitative in most cases, the intensity ratio between the two signals is 1:2, consistent with the corresponding number of C atoms. A shoulder can be observed at 22.7 ppm, which could be attributed to MPTMS not incorporated in the silica framework [30].

Assuming that the sulphur content determined by CHS elemental analysis is representative of the amount of incorporated MPTMS, the effectiveness of the functionalization procedure can be assessed. The nominal and the experimental sulphur amount for the SBA-15-SH sample were 14.68 and 5.75 wt%, respectively, which indicates

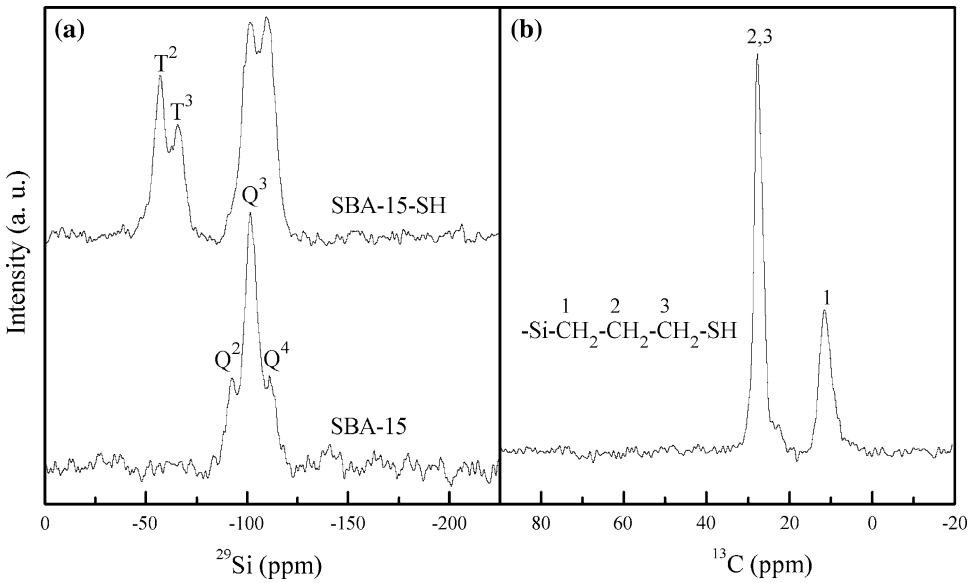

Fig. 4 ^{29}Si CPMAS NMR spectra of SBA-15 and SBA-15-SH (**a**), ^{13}C CPMAS NMR spectrum of SBA-15-SH (**b**)

that 39% of the functionalizing agent was incorporated in the silica structure.

Influence of the thermal treatments on the chemico-physical properties of Au/SBA-15-SH

The wide angle XRD patterns of Au/SBA-15-SH, as-made and after different thermal treatments, are represented in Fig. 5 and the corresponding Au mean particle diameters are reported in Table 1. The as-made sample (curve a) exhibits only the haloes typical of amorphous silica, indicating that gold is dispersed as small clusters. All the other samples show a series of crystalline peaks, which are due to the gold phase. The pattern of the sample calcined in air at 560 °C (curve b) exhibits Bragg reflections which, on the basis of their position and relative intensity, can unequivocally be ascribed to the face-centred cubic-phase of metallic gold (PDF 004-784). No peaks of any other phase are detected. The calculated average crystallite size is 5.7 nm. A limited growth of the particles (from 5.7 to 6.4 nm) occurs when the calcined sample is further treated at 600 °C in H_2/He atmosphere (curve d). It seems that the growth of the gold particles beyond this size is actually prevented by the confinement within the pore structure of SBA-15. Interestingly, treating the as-made sample at 600 °C in H_2/He (curve c) leads to the formation of small crystallites of 2.7 nm. The difference in the Au particle size between Au/SBA-15-SH calcined in air and Au/SBA-15-SH treated in H_2/He atmosphere can be interpreted by considering the different mode of MPTMS elimination. In the former case, combustion of the functionalizing agent leads to its complete removal. This was clearly shown by the lack of the signals at low field in the ^{29}Si CPMAS NMR

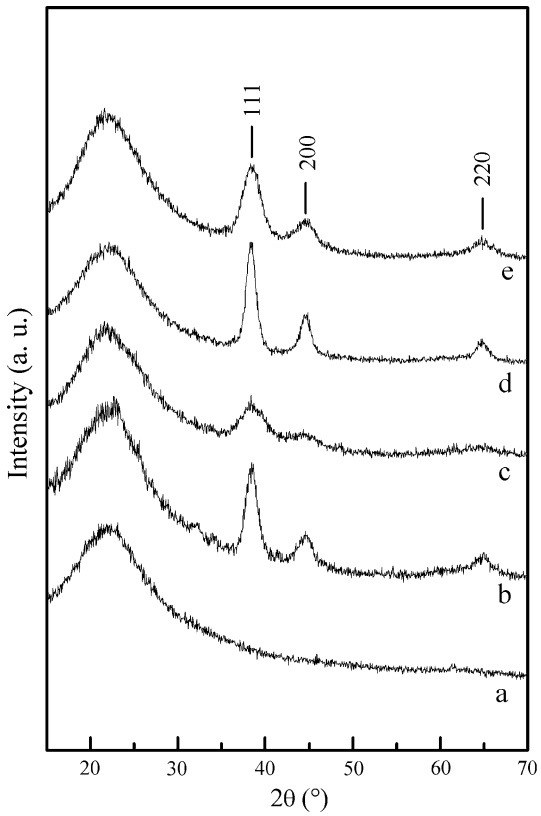

Fig. 5 Wide angle X-ray diffraction patterns of Au/SBA-15-SH: as-made (*a*) and after different thermal treatments: air 560 °C (*b*), H_2/He 600 °C (*c*), air 560 °C–H_2/He 600 °C (*d*), H_2/He 600 °C–air 560 °C–H_2/He 600 °C (*e*)

spectrum of the calcined sample (not shown), as well as by CHS analysis, which revealed no presence of S and only traces of C. In the case of the H_2-treated sample, MPTMS undergoes decomposition instead of combustion; this

Table 1 Mean diameters of gold nanoparticles from XRD results after different thermal treatments of the Au/SBA-15-SH sample

Thermal treatment	D_{XRD} (nm)
None	n.d.
Air 560 °C	5.7
H_2/He 600 °C	2.7
Air 560 °C–H_2/He 600 °C	6.4
H_2/He 600 °C–air 560 °C–H_2/He 600 °C	3.7

results in the presence of carbon residues on the surface, as previously found for similar samples [20]. It might be thought that the growth of the gold particles is somewhat limited by the presence of such carbon residues on the Au nanocrystals. When the H_2-treated sample is submitted to calcination at 560 °C followed by a second high-temperature treatment in H_2/He atmosphere (curve e), the gold particles grow from 2.7 to 3.7 nm. It hence appears that the treatment sequence H_2/He 600 °C–air 560 °C–H_2/He 600 °C is able to keep the gold particles' diameter well below the size of the SBA-15 pores.

The XRD results are confirmed by TEM analysis. No gold particles were visible in the as-made sample (not reported here), suggesting that gold is dispersed as clusters within the matrix. TEM bright field images are reported in Fig. 6 for the Au/SBA-15-SH catalyst after the following thermal treatments: (i) air 560 °C, (ii) air 560 °C–H_2/He 600 °C, (iii) H_2/He 600 °C–air 560 °C–H_2/He 600 °C. All samples show spherical gold nanoparticles homogeneously

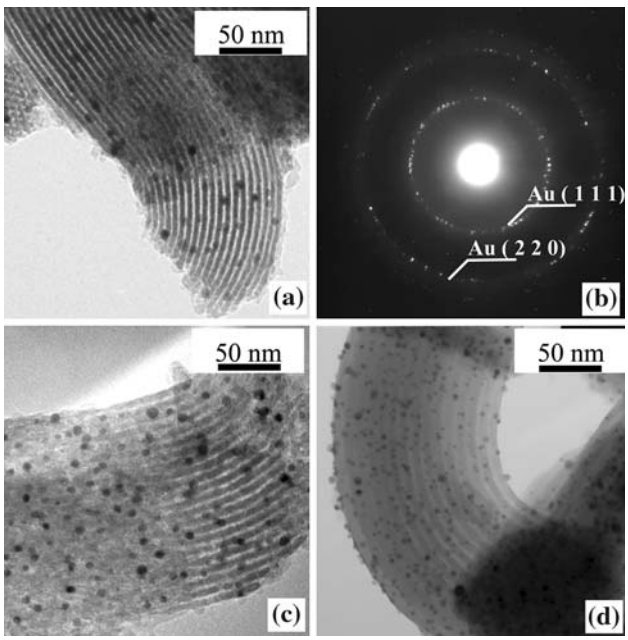

Fig. 6 TEM micrographs of Au/SBA-15-SH after different thermal treatments: air 560 °C (**a**), air 560 °C (SAD) (**b**), air 560 °C–H_2/He 600 °C (**c**), H_2/He 600 °C–air 560 °C–H_2/He 600 °C (**d**)

dispersed in the matrix, inside the pores and on the surface; only a low amount of gold is found as "free" nanoparticles. The gold particle size of the samples submitted to treatment (i) or (ii) is around 6 nm (Fig. 6a and c, respectively). After treatment (iii), tiny gold particles of about 4 nm are visible (Fig. 6d). The crystallinity and crystallography of the gold phase in the thermally treated samples were also investigated by selected area electron diffraction (SAD). The diffraction rings were found to correspond to the main d-spacing of the cubic gold phase. The SAD image of the sample after treatment (i) is reported in Fig. 6b as an example.

The FTIR spectra of Au/SBA-15-SH, as-made and after different thermal treatments, were collected after CO adsorption at −196 °C. As expected, the as-prepared sample outgassed at room temperature or at 150 °C (to remove adsorbed water) showed no signals due to CO adsorption (spectra not reported): because of its strong interaction with the mercapto group of MPTMS, gold is unable to adsorb CO. The FTIR spectrum of Au/SBA-15-SH after calcination in O_2 at 560 °C (Fig. 7a) shows two main peaks at 2156 and 2138 cm^{-1}, which can be ascribed to CO interacting with isolated silanols and to "liquid-like" CO (because of its condensation within the SBA-15 micropores), respectively. Besides these bands, for the lowest CO coverage, a further component can be observed as a shoulder at 2132 cm^{-1}, which can be ascribed to $Au^{\delta+}$–CO species. Such component was better observed in the case of adsorption of CO at room temperature (spectra in the inset), when CO condensation within the SBA-15 micropores does not occur. The formation of $Au^{\delta+}$ sites located at the surface of gold particles has been reported for Au/TiO_2 samples heated in the presence of oxygen [31]. CO adsorbed on these sites was characterized by frequencies in the 2154–2116 cm^{-1} region, lower than that reported for Au^{+}–CO species (2175–2160 cm^{-1}). Such $Au^{\delta+}$ sites were assumed to form as a consequence of the oxidation of surface gold atoms and the subsequent electron transfer from the Au particles to the Au^{+} species. According to this view, the lack of signals ascribable to Au^{0}-CO interactions (Fig. 7a) is not surprising. Figure 7b shows the spectra of CO adsorbed on the sample treated in H_2 at 600 °C. At low equilibrium pressures, a band at 2170 cm^{-1} is observed, ascribed to CO interacting with isolated Au^{+} ions. At higher coverage, the band shifts towards lower frequencies. This may be due to some heterogeneity in the Au^{+} sites. The overlap with the increasing component due to CO interacting with Si–OH species at 2156 cm^{-1} may also account for the downward shift of the maximum. It can be noted that the band at 2138 cm^{-1} is markedly lower than in the case of the calcined sample; this may be ascribed to the filling of the SBA-15 micropores by carbon residues coming from MPTMS decomposition.

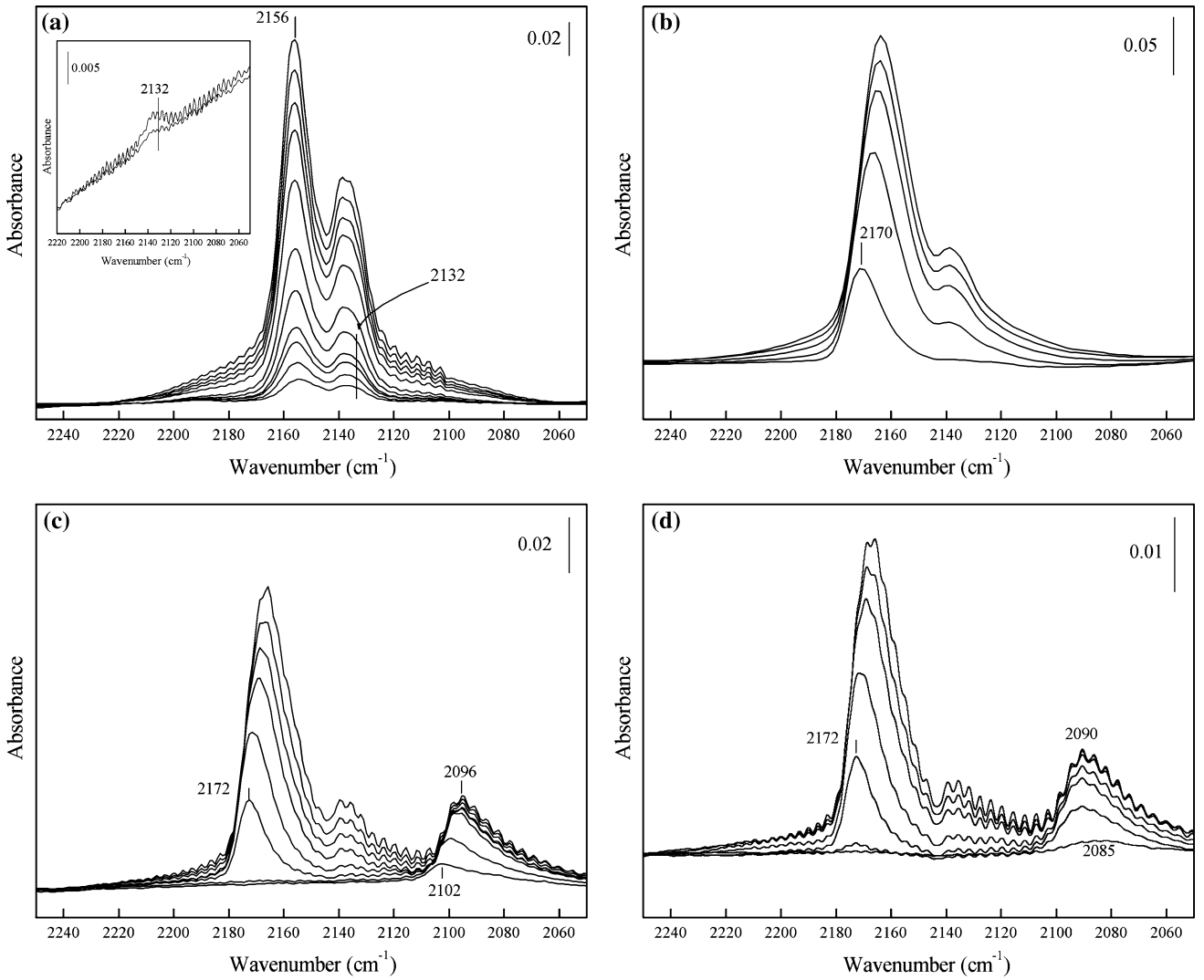

Fig. 7 FTIR spectra of CO adsorbed at −196 °C on Au/SBA-15-SH after different thermal treatments: O_2 560 °C (**a**), H_2 600 °C (**b**), O_2 560 °C–H_2 600 °C (**c**), H_2 600 °C–O_2 560 °C–H_2 600 °C (**d**). Inset in (**a**): FTIR spectra of CO adsorbed at room temperature on Au/SBA-15-SH after treatment in O_2 at 560 °C

Carbon residues would also hinder the establishing of Au^0–CO interactions, which would also explain the lack of the corresponding signals in Fig. 7b. Figure 7c shows the spectrum of Au/SBA-15-SH after calcination in O_2 at 560 °C followed by H_2 treatment at 600 °C. The band at 2172 cm^{-1} due to CO adsorbed on Au^+ cations is clearly visible; also in this case a shift towards lower frequencies occurs with increasing coverage. At the lowest equilibrium pressure, a band appears at 2102 cm^{-1}, which shifts towards lower frequencies (2096 cm^{-1}) and becomes broader at increasing coverage. This band can be ascribed to CO adsorbed on Au^0 sites, as already reported for Au/Al_2O_3 catalysts [32]. It can be inferred that the H_2 treatment reduces the $Au^{\delta+}$ species (previously formed during the exposure to oxygen) to Au^0. Figure 7d shows the spectra of the sample submitted to the following treatment: H_2 600 °C–O_2 560 °C–H_2 600 °C. They are similar to those obtained after the sequence O_2 560 °C–H_2 600 °C (Fig. 7c), though the band ascribed to the Au^0 sites is overlapped to a component at slightly lower frequencies, visible at 2085 cm^{-1} at the lowest coverage, which can be assigned to CO molecules interacting with Au^- species [33]. FTIR frequencies of CO adsorbed on gold species after different thermal treatments are summarized in Table 2.

Catalytic activity

The as-made sample resulted inactive in the investigated range of temperatures (40–150 °C). CO conversion versus reaction temperature for the differently treated Au/SBA-15-SH samples is presented in Fig. 8; both conversion and turnover frequency (TOF) at 40 and 80 °C are listed in Table 3. Figure 8 shows that CO conversion is extremely

Table 2 FTIR frequencies of CO adsorbed on gold species after different thermal treatments of the Au/SBA-15-SH sample

Thermal treatment	Frequencies (cm^{-1})			
	Au^{+}–CO	$Au^{\delta+}$–CO	Au^{0}–CO	Au^{-}–CO
O_2 560 °C		2132		
H_2 600 °C	2170			
O_2 560 °C–H_2 600 °C	2172		2102 – 2096	
H_2 600 °C–O_2 560 °C–H_2 600 °C	2172		2090	2085

low on the samples thermally treated either in air at 560 °C or under H_2/He atmosphere at 600 °C. An appreciable catalytic activity is observed for the catalysts (i) first calcined and then H_2 treated at high temperatures or (ii) exposed to the H_2/He atmosphere at 600 °C prior to the high temperature calcination and subsequent H_2 treatment: at 40 °C, CO conversion of 12 and 21 mol% is observed, respectively. Since the TOF values for these samples are quite similar (Table 3), the difference in their conversion is due to the different gold dispersion.

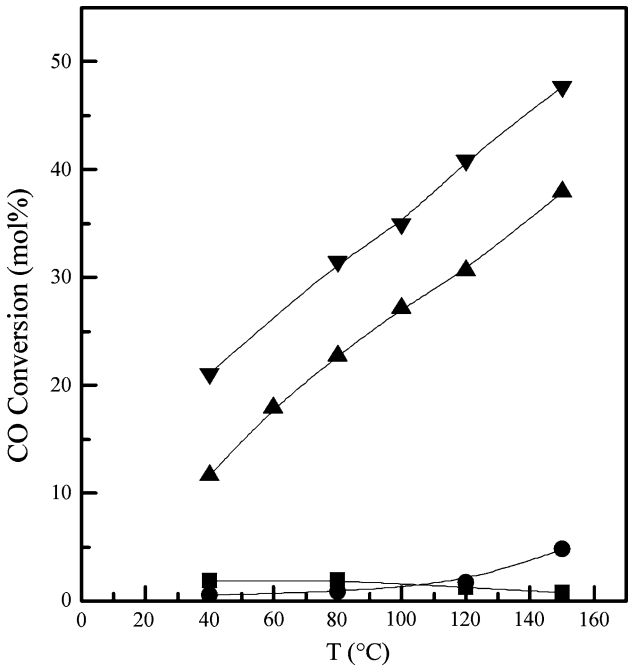

Fig. 8 CO conversion versus reaction temperature for Au/SBA-15-SH after different thermal treatments: air 560 °C (*black square*), H_2/He 600 °C (*black circle*), air 560 °C–H_2/He 600 °C (*black up-pointing triangle*), H_2/He 600 °C–air 560 °C–H_2/He 600 °C (*black down-pointing triangle*)

It is often assumed that for silica-supported gold catalysts, the catalytic activity is directly related to the Au particle size: due to the "inertness" of the support, gold particles of ca. 2 nm [35] would be required in order to activate both O_2 and CO on the metal. Present results indicate however that catalysts with gold nanocrystals beyond this size are also active, provided that a thermal pre-treatment under H_2/He atmosphere is carried out prior to reaction and the active sites are completely free from any organic residues (which in turn is achieved by calcination at high temperature). This adds further evidence to the view, first proposed in [12] and confirmed by recent results from the present authors' laboratory [20], that, as a consequence of the H_2 treatment, the usually considered "inert" silica undergoes "activation". This involves the formation of E' centres on the silica surface [12, 20], which hence becomes able to interact with the oxygen of the reaction atmosphere and to supply it to the CO molecule adsorbed on gold, thus allowing the oxidation reaction to occur.

The nature of the Au species able to adsorb CO and activate it for the reaction is still debated in the literature. Only Au^0 species have been proposed to be responsible for the catalytic activity in the CO oxidation on Au/TiO_2 [36, 37] or Au/Fe_2O_3 [38]. Other authors have suggested that both Au cations and Au^0 species are involved as active sites on gold-based catalysts when TiO_2 and Fe_2O_3 [39], Al_2O_3 [40] or NaY [41] are used as supports. The FTIR evidence obtained in the present work shows that Au^+ and Au^0 species able to adsorb CO are simultaneously present

Table 3 Catalytic performance of the Au/SBA-15-SH sample for the low temperature CO oxidation reaction

Thermal treatment	Conversion (mol%)		TOF (s^{-1})[a]	
	40 °C	80 °C	40 °C	80 °C
Air 560 °C	1.85	1.96	$1.11 \cdot 10^{-2}$	$1.17 \cdot 10^{-2}$
H_2/He 600 °C	0.55	0.87	$1.57 \cdot 10^{-3}$	$2.46 \cdot 10^{-3}$
Air 560 °C–H_2/He 600 °C	11.60	22.74	$7.80 \cdot 10^{-2}$	$1.53 \cdot 10^{-1}$
H_2/He 600 °C–air 560 °C–H_2/He 600 °C	21.13	31.47	$8.21 \cdot 10^{-2}$	$1.22 \cdot 10^{-1}$

[a] TOF was calculated by using the relationship between the metal dispersion and the mean particle size reported in [34]

(Fig. 7c, d) on the active catalysts. It is worthy to note that the presence of Au^{+} alone does not result in an active catalyst, though such species are able to interact with carbon monoxide (Fig. 7b). The conclusion can be drawn that Au^{0} is required for the activation of CO. Further experimental work is needed in order to understand the role of the Au^{+} species. At variance with the above catalysts, "activation" of the support has not occurred for the calcined Au/SBA-15-SH sample. Accordingly, nothing can be said on the role of the $Au^{\delta+}$ species observed on such catalyst (Fig. 7a).

Conclusions

Gold can be atomically dispersed within the pores of SBA-15, provided that its surface has been functionalized. Due to the strong interactions between Au and the functionalizing agent, such system is catalytically inactive for low temperature CO oxidation.

High temperature calcination is needed in order to completely remove the functionalizing agent. This treatment results in gold nanoparticles of ca. 6 nm, too large for being catalytically active.

Further treatment under H_2 leads to an active catalyst, in spite of the size of the Au nanoparticles. This confirms that the silica support is directly involved in the activation of the reactant oxygen.

The H_2 treatment causes a slight increase in the diameter of the Au particles, which however do not grow beyond the size of the pores of the support. SBA-15 is hence effective in limiting the growth of the gold nanocrystals.

Small Au particles (3.7 nm) can be obtained by thermally treating the sample first under H_2/He, then under air and finally under H_2/He again. As a consequence, the CO conversion for the resulting catalyst is higher than for the sample only treated under air and H_2/He. The TOF values for the two catalysts are similar, which indicates that the different conversion values stem from the different gold dispersion.

FTIR analysis reveals that on the active catalysts Au^{0} and Au^{+} species are able to adsorb CO. When CO adsorbs on Au^{+} sites only, no catalytic activity is observed. It hence seems that adsorption on Au^{0} species is needed for carbon monoxide activation and reaction. No safe conclusion can be drawn on the role of the Au^{+} species.

References

1. Haruta M, Yamada N, Kobayashi T, Iijima S (1989) J Catal 115:301
2. Haruta M, Tsubota S, Kobayashi T, Kageyama H, Genet MJ, Delmon B (1993) J Catal 144:175
3. Yuan Y, Kozlova AP, Asakura K, Wan H, Tsai K, Iwasawa Y (1997) J Catal 170:191
4. Okumura M, Nakamura S, Tsubota S, Nakamura T, Azuma M, Haruta M (1998) Catal Lett 51:53
5. Grunwaldt J-D, Maciejewski M, Becker OS, Fabrizioli P, Baiker A (1999) J Catal 186:458
6. Grisel RJH, Nieuwenhuys BE (2001) J Catal 199:48
7. Wolf A, Schüth F (2002) Appl Catal A Gen 226:1
8. Mallick K, Scurrel MS (2003) Appl Catal A Gen 253:527
9. Yang C, Kalwei M, Schüth F, Chao K (2003) Appl Catal A Gen 254:289
10. Rossignol C, Arrii S, Morfin F, Piccolo L, Caps V, Rousset J-L (2005) J Catal 230:476
11. Russo N, Fino D, Saracchio G, Specchia V (2006) Catal Today 117:214
12. Chiang C-W, Wang A, Mou C-Y (2006) Catal Today 117:220
13. Avgouropoulos G, Manzoli M, Boccuzzi F, Tabakova T, Papavasiliou J, Ioannides T, Idakiev V (2008) J Catal 256:237
14. Qian K, Huang WX, Fang J, Lv SS, He B, Jiang ZQ, Wei SQ (2008) J Catal 255:269
15. Zhao D, Feng J, Huo Q, Melosh N, Fredrickson GH, Chmelka BF, Stucky GD (1998) Science 279:548
16. Guari Y, Thieuleux C, Mehdi A, Reyé C, Corriu RJP, Gomez-Gallardo S, Philippot K, Chaudret B (2003) Chem Mater 15:2017
17. Yang C, Liu P, Ho Y, Chiu C, Chao K (2003) Chem Mater 15:275
18. Ghosh A, Patra CR, Mukherjee P, Sastry M, Kumar R (2003) Microporous Mesoporous Mater 58:201
19. Bore MT, Pham HN, Switzer EE, Ward TL, Fukuoka A, Datye AK (2005) J Phys Chem B 109:2873
20. Rombi E, Cutrufello MG, Cannas C, Casu M, Gazzoli D, Occhiuzzi M, Monaci R, Ferino I (2009) Phys Chem Chem Phys 11:593
21. Martin T, Galarneau A, Brunel D, Izard V, Hulea V, Blanc AC, Abramson S, Di Renzo F, Fajula F (2001) Stud Surf Sci Catal 135:178
22. Lindlar B, Lüchinger M, Röthlisberger A, Haouas M, Pirngruber G, Kogelbauer A, Prins R (2002) J Mater Chem 12:528
23. Klug HP, Alexander LE (1962) X ray diffraction procedures. Wiley, New York
24. Gobin OC, Wan Y, Zhao D, Kleitz F, Kaliaguine S (2007) J Phys Chem C 111:3053
25. Kim TW, Kleitz F, Ryoo R (2005) J Am Chem Soc 127:7601
26. Ciesla U, Schüth F (1999) Microporous Mesoporous Mater 27:131
27. Lipmaa E, Magi M, Samson A, Engelhardt G, Grimmer AR (1980) J Am Chem Soc 102:4889
28. Llusar M, Monros G, Roux C, Pozzo JL, Sanchez C (2003) J Mater Chem 13:2505
29. Wang YQ, Yang CM, Zibrowius B, Spliethoff B, Linden M, Schüth F (2003) Chem Mater 15:5029
30. Kao H-M, Shen T-Y, Wu J-D, Lee L-P (2008) Microporous Mesoporous Mater 110:461
31. Klimev Hr, Fajerwerg K, Chakarova K, Delannoy L, Louis C, Hadjiivanov K (2007) J Mater Sci 42:3299. doi:10.1007/s10853-006-0777-1
32. Centeno MA, Hadjiivanov K, Tz Venkov, Hr Klimev, Odriozola JA (2006) J Mol Catal A Chem 252:142
33. Mihaylov M, Gates BC, Fierro-Gonzales JC, Hadjiivanov K, Knözinger H (2007) J Phys Chem C 111:2548
34. Anderson JR (1975) Structure of metallic catalysts. Academic Press, London
35. Schubert MM, Hackenberg S, Van Veen AC, Muhler M, Plzak V, Behm RJ (2001) J Catal 197:113
36. Bollinger MA, Vannice MA (1996) Appl Catal B Environ 8:417

37. Liu H, Kozlov AI, Kozlova AP, Shido T, Asakura K, Iwasawa Y (1999) J Catal 185:252
38. Liu H, Kozlov AI, Kozlova AP, Shido T, Iwasawa Y (1999) Phys Chem Chem Phys 1:2851
39. Bond GC, Thompson DT (2000) Gold Bull 33:41
40. Costello CK, Kung MC, Oh H-S, Wang Y, Kung HH (2002) Appl Catal A Gen 232:159
41. Fierro-Gonzales JC, Gates BC (2004) J Phys Chem B 108:16999